BIOCHEMISTRY
including biophysical chemistry & molecular biology
Article

Biochemistry **2009,** *48,* 6805–6810 6805
DOI: 10.1021/bi900832t

Crystal Structure of an Archaeal Rad51 Homologue in Complex with a Metatungstate Inhibitor†

Yang Li, Yujiong He, and Yu Luo*

Department of Biochemistry, University of Saskatchewan, A3 Health Sciences Building, 107 Wiggins Road, Saskatoon, Saskatchewan, Canada S7N 5E5

Received May 14, 2009; Revised Manuscript Received June 19, 2009

ABSTRACT: Archaeal RadAs are close homologues of eukaryal Rad51s (~40% sequence identities). These recombinases promote a hallmark strand exchange process between homologous single-stranded and double-stranded DNA substrates. This DNA-repairing function also plays a key role in cancer cells' resistance to chemo- and radiotherapy. Inhibition of the strand exchange process may render cancer cells more susceptible to therapeutic treatment. We found that metatungstate is a potent inhibitor of RadA from *Methanococcus voltae*. The tungsten cluster binds RadA in the axial DNA-binding groove. This polyanionic species appears to inhibit RadA by locking the protein in its inactive conformation.

Homologous recombination plays a pivotal role in the repair of double-stranded DNA breaks and restart of stalled replication forks (*1*−*5*). A central DNA strand exchange process between a single-stranded DNA (ssDNA)[1] and a homologous double-stranded DNA (dsDNA) in homologous recombination is promoted by a superfamily of strand exchange proteins (also called recombinases) (*6*) including bacterial RecA (*7*), archaeal RadA (*8*), and eukaryal Rad51 (*9*) and DMC1 (*10*). Mammalian Rad51 is critical for development of embryos (*11*) and DNA repair (*12*). A small molecular compound has recently been identified to enhance Rad51's strand exchange activity (*13*). Potentially, this could serve as a drug to boost DNA repair. On the other hand, tumor cells tend to have an elevated level of Rad51 expression which correlates with their resistance to radio- and chemotherapies as reviewed (*14*). Therefore, a Rad51 inhibitor would serve as a potential adjuvant for cancer therapy.

Despite large differences between the bacterial and nonbacterial strand exchange proteins in their primary structures (less than 30% sequence identity), electron microscopic and crystallographic results have revealed strikingly similar filamentous assemblies (*15*−*20*). Three functionally important sites are notably conserved in these filamentous structures. The first is the polymerization motif which contains a central hydrophobic residue which matches a hydrophobic pocket in an adjacent subunit (*21*). This motif appears to exist in tandem in BRCA2 which recruits Rad51 to the site of DNA lesion (*22*). The second is the ATPase center located at the intersubunit interface which binds, hydrolyzes ATP, and regulates the conformation of the third conserved site of DNA binding. The conformation-switching role of the ATPase center has been visualized in crystal structures of MvRadA (*23*, *24*) and EcRecA (*19*). The DNA-interacting role of loops L1 and L2 was first suggested by the crystal structure of EcRecA (*15*). The larger L2 has two universally conserved residues at each end. In MvRadA, the four invariant residues are Asn-256, Gln-257, Gly-274, and Gly-275. The smaller L1 is not highly conserved between bacterial RecAs and nonbacterial RadA/Rad51/DMC1 homologues. Within the latter group, L1 has five conserved residues equivalent to Arg-218, Gly-223, Arg-224, Leu-227, and Arg-230 of MvRadA. Two of the three invariant arginine residues define the boundary of L1. The two disordered loops are located near the filament axis in this first crystal structure of EcRecA in an apparently inactive conformation. They become ordered in the active form of EcRecA in complex with ADP-AlF_4 and DNA (*19*). As expected, the two loops as well as ~10 residues at the C-terminal flank of L1 bind DNA. Although a structure of a nonbacterial recombinase in complex with DNA is yet to be determined, the structural similarities between the bacterial and nonbacterial recombinases suggest that L1 and L2 regions in the nonbacterial homologues are the most likely site of DNA interaction.

Theoretically, Rad51 and its homologues can be inhibited by targeting the three functionally important sites: recruitment and polymerization, ATP binding, and DNA binding. The ATPase center of EcRecA has been targeted by nucleotide analogues (*25*, *26*). However, there is no report on inhibitory compounds

†This work is supported by Canadian Institute of Health Research Operating Grant 63860 to Y.L. Some of the crystallographic study described in this paper was performed at the Canadian Light Source, which is supported by NSERC, NRC, CIHR, and the University of Saskatchewan.

*Corresponding author. Tel: 306-966-4379. Fax: 306-966-4390. E-mail: Yu.Luo@usask.ca.

[1]Abbreviations: MvRadA, RadA recombinase from *Methanococcus voltae*; EcRecA, RecA recombinase from *Escherichia coli*; ssDNA, single-stranded DNA; dsDNA, double-stranded DNA; hdDNA, heteroduplex DNA; ATP, adenosine 5′-triphosphate; ADP, adenosine 5′-diphosphate; AMP-PNP, 5′-adenylyl imidodiphosphate, a nonhydrolyzable analogue of ATP; FAM, fluorescein phosphoamidite; IPTG, isopropyl β-D-1-thiogalactopyranoside.

Published on Web 06/25/2009

which block the recruitment, polymerization, or DNA binding of strand exchange proteins. Since DNA is a polymer, it is not clear whether a much smaller molecule can effectively compete with DNA for binding Rad51. In our attempt to obtain a crystallographic snapshot of post-ATP hydrolysis conformation, we accidentally found that metatungstate is a potent inhibitor of ATPase and strand exchange activities of the archaeal Rad51 homologue from *Methanococcus voltae*. The tungsten cluster appears to be bound between the DNA-binding loops L1 and L2 anchoring the protein in its inactive conformation. The results suggest that competitive inhibition of DNA binding by Rad51 is possible.

EXPERIMENTAL PROCEDURES

Protein Preparation and Crystallization. The chemicals were purchased from VWR unless specified otherwise. The recombinant RadA protein from *M. voltae* was overexpressed and purified as reported MvRadA (*18*, *27*). The purified MvRadA protein was concentrated to ~30 mg/mL by ultrafiltration. The hexagonal MvRadA crystals ($P6_1$ space group) were grown by the hanging drop vapor diffusion method and grew to a maximum dimension of 0.1 mm × 0.1 mm × 0.3 mm in a few days. The protein sample contained ~1 mM MvRadA and 2 mM ADP. The reservoir solutions contained 6−8% polyethylene glycol 3350, 50 mM $MgCl_2$, 2 mM Na_2WO_4 or 0.5 mM $Na_6H_2W_{12}O_{40}$, 50 mM Tris-HCl buffer at pH 7.9, and 0.2−0.5 M NaCl. The crystals were transferred into a stabilizing solution composed of the reservoir solution supplemented with 28% (w/v) sucrose, looped out of the solution, and frozen in a nitrogen cryostream at 100 K. The diffraction data sets were collected first using an in-house Brukers Proteum system at a wavelength of 1.54 Å and later using synchrotron radiation at a wavelength of 0.97 Å. The synchrotron data sets were processed using the HKL-2000 program (HKL Research, Inc.). The statistics of the diffraction data are listed in Table 1.

Structural Determination and Refinement. The previously solved MvRadA model (PDB code 1T4G) was used as the starting model for rigid body refinement. The positions of tungsten atoms were located by high-density peaks in the anomalous difference map. Oxygen atoms of the metatungstate were not seen. The model was iteratively rebuilt using XtalView (*28*) and refined using CNS (*29*). Statistics of the refinement and model geometry are also given in Table 1. The molecular figures were generated using Molscript (*30*) and rendered using Raster3D (*31*). The coordinates and structure factors have been deposited in the Protein Data Bank (PDB entry 3FYH).

Strand Exchange Assay Using Synthetic Oligonucleotides. Three oligonucleotides (FAM43, 43 nt, FAM-TTTTG CGGAT GGCTT AGAGC TTAAT TGCTG AATCT GGTGC TGT; 45A, 36 nt, ACAGC ACCAG ATTCA GCAAT TAAGC TCTAA GCCATG; 55A, 36 nt, GATGG CTTAG AGCTT AATTG CTGAA TCTGG TGCTGT) were obtained from Integrated DNA Technologies. Equal molarities of complementary oligonucleotides 45A and 55A were heated at 95 °C for 5 min and then slowly cooled to 21 °C to generate the 36 bp dsDNA substrate. The strand exchange solution was composed of 5 mM ATP (Sigma-Aldrich), 10 mM $MgCl_2$, 100 mM KCl, 50 mM Hepes−Tris buffer at pH 7.4, 5 μM MvRadA, 0.1% (v/v) 2-mercaptoethanol, 0.33 μM oligonucleotides (or 14 μM in nucleotides), and specified concentration of sodium metatungstate (Sigma-Aldrich). The 43 nt 5′-fluorescein-labeled ssDNA substrate (oligonucleotide FAM43) was preincubated at 37 °C with MvRadA for 1 min before adding the 36 bp dsDNA substrate. The reaction was stopped at 30 min by adding EDTA to a concentration of 20 mM and trypsin to a concentration of 1 μg/μL. After 10 min of proteolysis, 10 μL of sample was mixed with 5 μL of a loading buffer composed of 30% glycerol and then loaded onto a 17% acrylamide vertical gel. The SDS−PAGE was developed for ~1 h at 100 V. The fluorescent emission by the intrinsic fluorescein was recorded and quantified using a Kodak GelLogic 200 system.

Table 1: Data Collection and Refinement Statistics

PDB entry	3FYH
substrate	ADP and metatungstate
Data Collection	
space group	$P6_1$
cell dimensions	
a, *b*, *c* (Å)	83.16, 83.16, 106.85
α, *β*, *γ* (deg)	90, 90, 120
resolution (Å)	1.90 (1.98−1.90)[a]
R_{sym}	0.092 (0.420)
I/σ	12.9 (3.5)
completeness (%)	97.7 (89.6)
unique reflections	32232 (3591)
redundancy	11.3 (8.2)
Refinement	
resolution (Å)	20.0−1.90
no. of reflections	32232
R_{work}/R_{free}	0.200/0.227
no. of atoms	2464
protein	2322
ligand/ion	26
water	116
B-factors	35.8
protein	35.5
ligand/ion	46.0
water	40.7
root-mean-square deviations	
bond lengths (Å)	0.014
bond angles (deg)	1.73

[a] Values in parentheses are for the highest-resolution shell.

ATPase Assay. A solution containing 0.033% (w/v) Malachite Green, 1.3% (w/v) ammonium molybdate, and 1.0 M HCl was used to monitor the release of inorganic phosphate (*32*) by ATP hydrolysis. Absorbance at 620 nm was recorded for quantification. The reaction solutions for the ssDNA-dependent ATPase assay contained 1 or 3 μM MvRadA, 6 or 18 μM ssDNA (in nucleotides), 5 mM ATP, 0.05 M Tris−Hepes buffer at pH 7.4, 100 mM KCl, 10 mM $MgCl_2$, 0.1% (v/v) 2-mercaptoethanol, and specified amount of sodium metatungstate. A 36 nt oligonucleotide poly$(dT)_{36}$ (Integrated DNA Technologies) was used as the ssDNA substrate. The reaction solutions were sampled at regular time intervals to monitor the liberated phosphate.

Single-Stranded Oligonucleotide-Binding Assay. The DNA-binding solution was identical to that in the strand exchange assay except that no dsDNA was present. The fluorescent oligonucleotide FAM43 (1 μM) and MvRadA (15 μM) were incubated for 10 min before loading onto a 2.0% agarose gel. The agarose gel was developed for 1 h at 100 V. The fluorescent emission by the intrinsic fluorescein was recorded and quantified using a Kodak GelLogic 200 system.

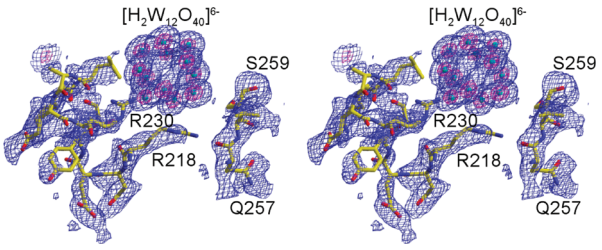

FIGURE 1: Electron density map in stereo. Omit ($F_o - F_c$) difference Fourier map at 1.9 Å resolution was contoured at 2σ in blue and 10σ in magenta. The metatungstate ion and ordered residues in the L1 region (residues 218−230) and the ordered N-terminal part of the L2 region (residues 257−259) are shown. The tungsten atoms are shown in cyan spheres. The C, N, and O atoms are colored in yellow, blue, and red, respectively.

Circular Single-Stranded Virion DNA-Binding Assay. The DNA-binding solution was identical to that in the FAM43-binding assay except for the concentrations of single-stranded ϕX174 virion DNA (New England Biolabs) and protein. The circular virion DNA (20 μM in nucleotides) and MvRadA (7 μM) were incubated for 10 min before loading onto a 1.0% agarose gel. The agarose gel was developed for 1 h at 100 V. The fluorescent emission by DNA-absorbed ethidium bromide was recorded and quantified by a Kodak GelLogic 200 system.

Double-Stranded DNA-Binding Assay. The DNA-binding solution was identical to that in the FAM43-binding assay except for the concentrations of DNA and protein. The double-stranded DNA was a 1.0 kb PCR product using ϕX174 virion DNA as the template. The linear dsDNA (30 μM in nucleotides) and MvRadA (10 μM) were incubated for 10 min before loading onto a 1.0% agarose gel. The agarose gel was developed for 1 h at 100 V. The fluorescent emission by DNA-absorbed ethidium bromide was recorded and quantified by a Kodak GelLogic 200 system.

RESULTS

Crystal Structure of MvRadA in Complex with ADP and Metatungstate. The MvRadA protein readily crystallizes in the presence of AMPPNP or ADP as reported (*18*, *24*). When we attempted to capture the posthydrolysis state by cocrystallizing in the presence of ADP and sodium tungstate (Na_2WO_4) as a phosphate analogue, a cluster of 12 tungsten atoms was unexpectedly located by outstanding anomalous scattering signals (data not shown) near the DNA-binding loops 1 and 2. We reasoned that the tungsten cluster seen in the crystal may be metatungstate, a compound known to form from tungstate in aqueous solution. When sodium metatungstate ($Na_6H_2W_{12}O_{40}$) was used as the substitute for tungstate, an essentially identical electron density map was indeed observed (Figure 1). The polyanionic metatungstate is located near the filament axis of the crystallized MvRadA (Figure 2A). It is in contact with both Arg-218 and Arg-230 in the L1 region of MvRadA (Figures 1 and 2B). The third invariant Arg-224 in nonbacterial RecA homologues was disordered in the crystal. At least 1 of the 12 tungsten atoms was observed in close proximity (within 5 Å) of residues Thr-222 and Ser-259 as well as residues Ala-228 and Gln-232 of a nearby protomer (not shown). The L2 region is largely disordered with no interpretable electron density for residues 260−278. The invariant His-280 in nonbacterial RecA homologues is distant from the ATP analogue. These structural features appear to suggest that the metatungstate-bound MvRadA is in its inactive

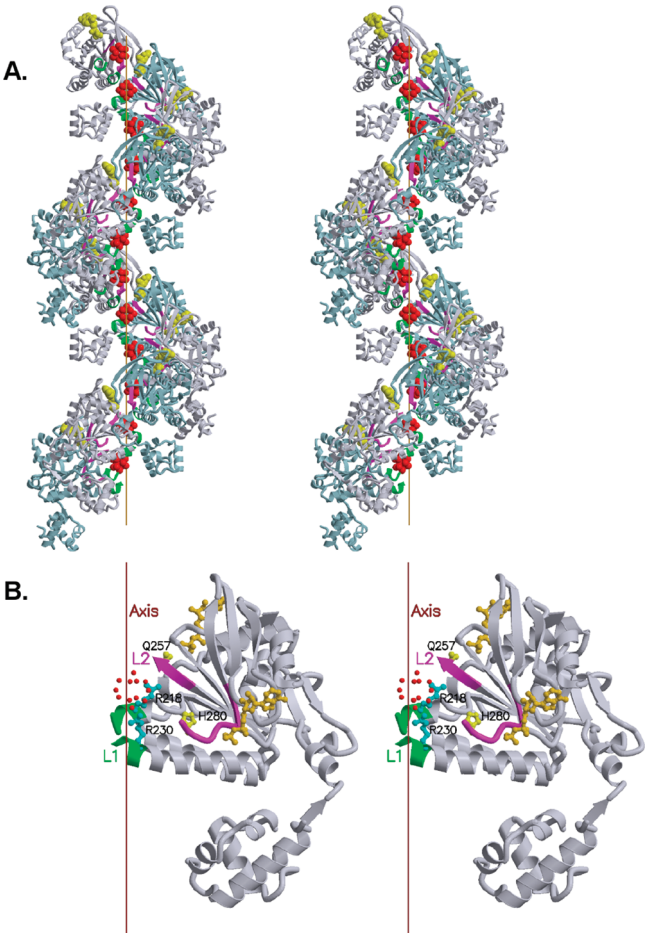

FIGURE 2: Structure of MvRadA/ADP/metatungstate complex in stereo. Ribbons of MvRadA monomers are shown in alternating gray and light blue. The ordered parts of the L1 and L2 regions are highlighted in green and magenta, respectively. The filament axis is shown. The ADP molecules are shown in yellow. The tungsten atoms are shown in red. (A) The crystallized filament. (B) One MvRadA monomer. The side chains of ATP-interacting residues Gln-257 and His-280 are shown in yellow sticks. The side chains of DNA-interacting residues Arg-218 and Arg-230 are shown in cyan sticks.

conformation as previously reported (*18*, *24*). We then repeatedly attempted the crystallization conditions in the presence of KCl or $CaCl_2$ which have been known to crystallize MvRadA in its ATPase-active conformation (*23*, *33*). Although the crystals readily formed in the presence of metatungstate, the tungsten cluster was never seen in the electron density map. It appears that the binding of metatungstate in the crystal is incompatible with the active conformation. Structural comparison further suggests that residues around Ser-259 seen in the ATPase-active conformation of MvRadA (*23*) would cause steric clash with the recombinase-bound metatungstate.

Metatungstate Inhibits DNA Strand Exchange Promoted by MvRadA. Since metatungstate is bound at the site near both L1 and L2 (Figure 2), it should compete with DNA for binding MvRadA. As expected, the strand exchange process was inhibited by sodium metatungstate (Figure 3). A concentration of 4 μM metatungstate completely inhibited the strand exchange process promoted by 5 μM MvRadA.

Metatungstate Inhibits ATP Hydrolysis. The crystal structure of MvRadA also suggests that the metatungstate-bound state resembles the inactive state of MvRadA. We expected that metatungstate should also inhibit ATP hydrolysis

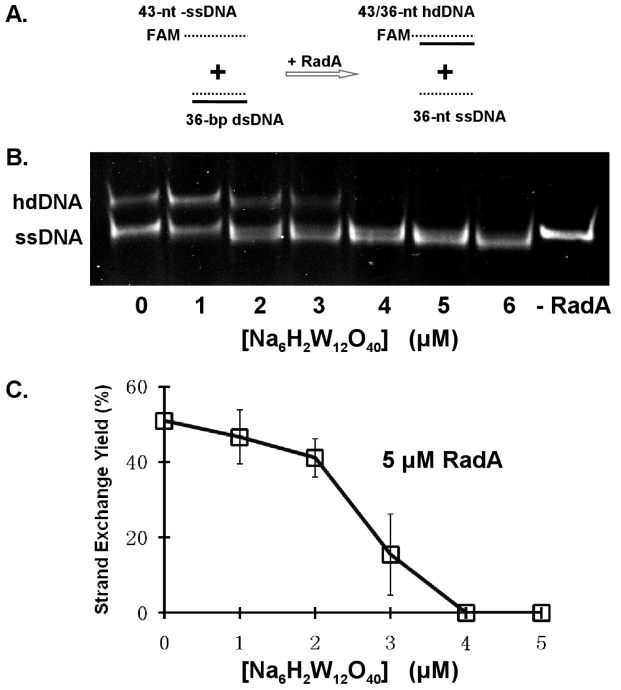

FIGURE 3: Inhibition of DNA strand exchange activity of MvRadA. The strand reaction scheme is shown in (A). The reaction solutions contained 5 mM ATP, 10 mM $MgCl_2$, 100 mM KCl, 50 mM Hepes−Tris buffer at pH 7.4, 5 μM MvRadA, 0.1% (v/v) 2-mercaptoethanol, 0.33 μM oligonucleotides (or 14 μM in nucleotides or base pairs), and specified concentration of sodium metatungstate (Sigma-Aldrich). Strand exchange activity was indicated by the formation of the slowest migrating heteroduplex DNA species (FAM-labeled hdDNA). The intrinsic fluorescence from the FAM label was recorded as shown in (B). The quantified strand exchange yields and standard deviations from five repeated experiments are shown in (C).

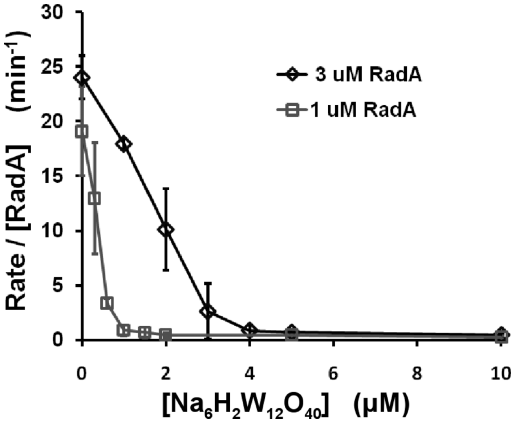

FIGURE 4: Inhibition of ATPase activity of MvRadA. The reaction solutions contained 5 mM ATP, 10 mM $MgCl_2$, 100 mM KCl, 50 mM Hepes−Tris buffer at pH 7.4, 0.1% (v/v) 2-mercaptoethanol, and specified concentration of sodium metatungstate (Sigma-Aldrich). Quantified results were derived from three repeated experiments. The reaction also contained 18 μM (in nucleotides) poly(dT)$_{36}$ and 3 μM MvRadA or 6 μM poly(dT)$_{36}$ and 1 μM MvRadA.

catalyzed by MvRadA. When 3 μM MvRadA was used, an equal molarity of metatungstate caused an ~90% decrease in ATP hydrolysis (Figure 4). Since the ATP hydrolysis assay is more sensitive than the DNA strand exchange assay, we were able to get quantitative results using a lower MvRadA concentration of 1 μM. Again, MvRadA-catalyzed ATP hydrolysis was efficiently inhibited by an equal amount of metatungstate (Figure 4).

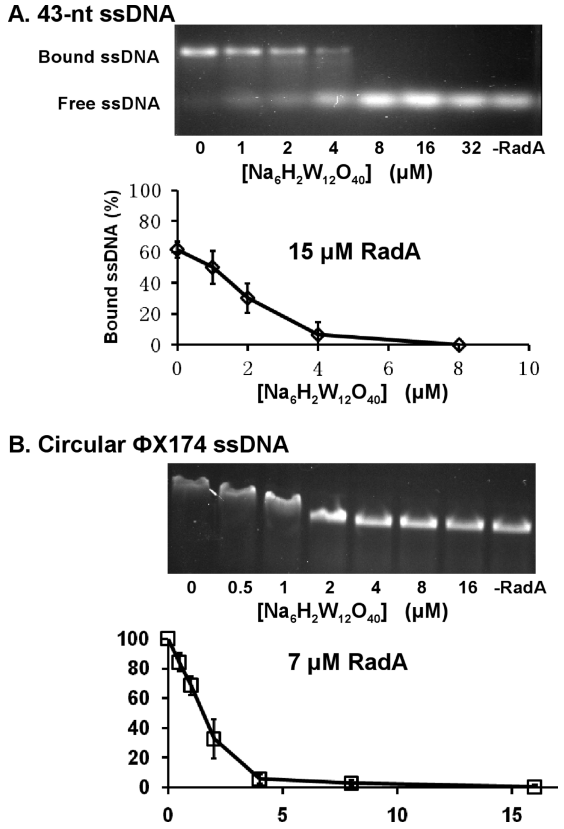

FIGURE 5: Inhibition of ssDNA binding. The reaction solutions contained 5 mM ATP, 10 mM $MgCl_2$, 100 mM KCl, 50 mM Hepes−Tris buffer at pH 7.4, 0.1% (v/v) 2-mercaptoethanol, and specified concentration of sodium metatungstate (Sigma-Aldrich). Quantified results were derived from five repeated experiments. (A) The reaction also contained 1 μM FAM43 (or 43 μM in nucleotides) and 15 μM MvRadA. (B) The reaction also contained 20 μM circular ϕX174 ssDNA (in nucleotides) and 7 μM MvRadA.

Metatungstate Inhibits ssDNA Binding. We further resorted to DNA-binding assays to study the inhibitory effect of metatungstate. For the 43 nt single-stranded synthetic oligonucleotide in the presence of 15 μM MvRadA, the binding of RadA appeared to be an all-or-none process (Figure 5A). A slower gel band corresponded to the RadA-coated oligonucleotide. When 8 μM or more metatungstate was present, the RadA-bound DNA band disappeared.

When circular single-stranded ϕX174 DNA (5386 nt) and 7 μM MvRadA were used in the DNA binding assay (Figure 5B), only one DNA band was visible on the agarose gel. The migration rate of the DNA appeared to be dependent on the concentration of metatungstate. We reasoned that the nucleation events on such long ssDNA molecules may be relatively fast so that the degree of MvRadA coating becomes similar for each DNA molecule. Instead of using the integrated brightness of the bands for quantification, we used the relative rate of migration as the measure of bound fraction. Again, metatungstate appeared to be an effective inhibitor of ssDNA binding.

Metatungstate Inhibits dsDNA Binding. MvRadA did not appear to bind the 36 bp dsDNA in assays using up to 20 μM MvRadA. The protein-bound 1000 bp dsDNA in the presence of 10 μM MvRadA appeared as a slightly smeared slower migrating band (Figure 6). The presence of 4 μM metatungstate almost completely blocked the binding of this dsDNA.

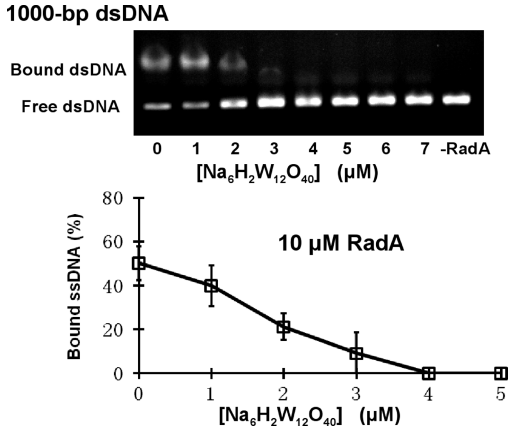

FIGURE 6: Inhibition of dsDNA binding. The reaction solutions contained 5 mM ATP, 10 mM $MgCl_2$, 100 mM KCl, 50 mM Hepes−Tris buffer at pH 7.4, 0.1% (v/v) 2-mercaptoethanol, and specified concentration of sodium metatungstate (Sigma-Aldrich). Quantified results were derived from five repeated experiments. The reaction also contained a 1000 bp dsDNA (30 μM in base pairs) and 10 μM MvRadA.

DISCUSSION

The metatungstate ion bound at the DNA-binding site appears to freeze MvRadA in its ATPase-inactive conformation, which further exemplifies the allosteric nature of the strand exchange protein. This has been confirmed by the compound's inhibitory effect on the ATPase activity of MvRadA. The location of the tungsten cluster between the putative DNA-binding loops L1 and L2 also suggests that the compound could competitively inhibit RadA-promoted DNA strand exchange. Our assays proved that metatungstate is a potent inhibitor of DNA strand exchange as well as DNA binding. The DNA strand exchange and ATPase assays appear to suggest that metatungstate is a quantitative inhibitor of MvRadA. The tungsten cluster belongs to a family of polyoxometalates. Many such compounds have been found to have anti-RNA virus activity (*34*). Some of these antiviral compounds have also been known to inhibit DNA binding by HIV-1 reverse transcriptase (*35*). Metatungstate stands out in polyoxometalates with the highest hexaanionic charges in solution. Its intense anionic nature may interact most favorably with the cationic surface of the DNA-binding region of the Rad51 homologue. In fact, two of the three invariant arginine residues in RadA/Rad51/DMC1 homologues (Arg-218 and Arg-230 of MvRadA) are in contact with the metatungstate ion. We also tested two similarly shaped but trianionic compounds (phosphotungstate and phosphomolybdate) using the ATPase assay. Similar IC_{50} values around 30 μM were derived (data not shown). Their lower inhibitory efficiency could be explained by their lesser anionic charge. Despite large differences in amino acid sequence, EcRecA also appeared to be inhibited by the three polyoxometalates (data not shown). Although the highly charged metatungstate is unlikely to permeate the cell membrane, our results exemplify the potential of any future Rad51 inhibitor which competes with DNA for binding Rad51. Such a future inhibitor would be important in studying the mechanism of cancer cells' resistance to radio- and chemotherapies and a potential adjuvant to such therapies. Design of a Rad51 inhibitor would probably focus on the utilization of the conserved feature of the archaeal/eukaryal Rad51 homologues such as the three cationic arginine residues. As such, a future drug-like organic inhibitor would likely form strong π−cation bonding (*36*, *37*) with Rad51 rather than the anion−cation interaction seen in the MvRadA/metatungstate complex.

ACKNOWLEDGMENT

We thank Drs. Gabriele Schatte, Michel Fodje, and Pawel Grochulski for assistance with the X-ray facilities at the Saskatchewan Structural Sciences Centre and the Canadian Light Source.

REFERENCES

1. Cox, M. M. (1998) A broadening view of recombinational DNA repair in bacteria. *Genes Cells 3*, 65–78.
2. Cox, M. M., Goodman, M. F., Kreuzer, K. N., Sherratt, D. J., Sandler, S. J., and Marians, K. J. (2000) The importance of repairing stalled replication forks. *Nature 404*, 37–41.
3. Courcelle, J., Ganesan, A. K., and Hanawalt, P. C. (2001) Therefore, what are recombination proteins there for? *BioEssays 23*, 463–470.
4. Lusetti, S. L., and Cox, M. M. (2002) The bacterial RecA protein and the recombinational DNA repair of stalled replication forks. *Annu. Rev. Biochem. 71*, 71–100.
5. Kowalczykowski, S. C. (2000) Initiation of genetic recombination and recombination-dependent replication. *Trends Biochem. Sci. 25*, 156–165.
6. Seitz, E. M., and Kowalczykowski, S. C. (2000) The DNA binding and pairing preferences of the archaeal RadA protein demonstrate a universal characteristic of DNA strand exchange proteins. *Mol. Microbiol. 37*, 555–560.
7. Clark, A. J., and Margulies, A. D. (1965) Isolation and characterization of recombination-deficient mutants of *Escherichia coli* K12. *Proc. Natl. Acad. Sci. U.S.A. 53*, 451–459.
8. Sandler, S. J., Satin, L. H., Samra, H. S., and Clark, A. J. (1996) recA-like genes from three archaean species with putative protein products similar to Rad51 and Dmc1 proteins of the yeast *Saccharomyces cerevisiae*. *Nucleic Acids Res. 24*, 2125–2132.
9. Shinohara, A., Ogawa, H., and Ogawa, T. (1992) Rad51 protein involved in repair and recombination in *S. cerevisiae* is a RecA-like protein. *Cell 69*, 457–470.
10. Bishop, D. K., Park, D., Xu, L., and Kleckner, N. (1992) DMC1: a meiosis-specific yeast homolog of *E. coli* recA required for recombination, synaptonemal complex formation, and cell cycle progression. *Cell 69*, 439–456.
11. Tsuzuki, T., Fujii, Y., Sakumi, K., Tominaga, Y., Nakao, K., Sekiguchi, M., Matsushiro, A., Yoshimura, Y., and Morita, T. (1996) Targeted disruption of the Rad51 gene leads to lethality in embryonic mice. *Proc. Natl. Acad. Sci. U.S.A. 93*, 6236–6240.
12. Taki, T., Ohnishi, T., Yamamoto, A., Hiraga, S., Arita, N., Izumoto, S., Hayakawa, T., and Morita, T. (1996) Antisense inhibition of the RAD51 enhances radiosensitivity. *Biochem. Biophys. Res. Commun. 223*, 434–438.
13. Jayathilaka, K., Sheridan, S. D., Bold, T. D., Bochenska, K., Logan, H. L., Weichselbaum, R. R., Bishop, D. K., and Connell, P. P. (2008) A chemical compound that stimulates the human homologous recombination protein RAD51. *Proc. Natl. Acad. Sci. U.S.A. 105*, 15848–15853.
14. Klein, H. L. (2008) The consequences of Rad51 overexpression for normal and tumor cells. *DNA Repair* (*Amsterdam*) *7*, 686–693.
15. Story, R. M., Weber, I. T., and Steitz, T. A. (1992) The structure of the *E. coli* recA protein monomer and polymer. *Nature 355*, 318–325.
16. VanLoock, M. S., Yu, X., Yang, S., Lai, A. L., Low, C., Campbell, M. J., and Egelman, E. H. (2003) ATP-mediated conformational changes in the RecA filament. *Structure* (*Cambridge*) *11*, 187–196.
17. Conway, A. B., Lynch, T. W., Zhang, Y., Fortin, G. S., Fung, C. W., Symington, L. S., and Rice, P. A. (2004) Crystal structure of a Rad51 filament. *Nat. Struct. Mol. Biol. 11*, 791–796.
18. Wu, Y., He, Y., Moya, I. A., Qian, X., and Luo, Y. (2004) Crystal structure of archaeal recombinase RadA: a snapshot of its extended conformation. *Mol. Cell 15*, 423–435.
19. Chen, Z., Yang, H., and Pavletich, N. P. (2008) Mechanism of homologous recombination from the RecA-ssDNA/dsDNA structures. *Nature 453*, 489–484.
20. Sheridan, S. D., Yu, X., Roth, R., Heuser, J. E., Sehorn, M. G., Sung, P., Egelman, E. H., and Bishop, D. K. (2008) A comparative analysis of Dmc1 and Rad51 nucleoprotein filaments. *Nucleic Acids Res. 36*, 4057–4066.

21. Pellegrini, L., Yu, D. S., Lo, T., Anand, S., Lee, M., Blundell, T. L., and Venkitaraman, A. R. (2002) Insights into DNA recombination from the structure of a RAD51-BRCA2 complex. *Nature 420*, 287–293.
22. Yang, H., Li, Q., Fan, J., Holloman, W. K., and Pavletich, N. P. (2005) The BRCA2 homologue Brh2 nucleates RAD51 filament formation at a dsDNA-ssDNA junction. *Nature 433*, 653–657.
23. Wu, Y., Qian, X., He, Y., Moya, I. A., and Luo, Y. (2005) Crystal structure of an ATPase-active form of Rad51 homolog from *Methanococcus voltae*. Insights into potassium dependence. *J. Biol. Chem. 280*, 722–728.
24. Qian, X., Wu, Y., He, Y., and Luo, Y. (2005) Crystal structure of *Methanococcus voltae* RadA in complex with ADP: hydrolysis-induced conformational change. *Biochemistry 44*, 13753–13761.
25. Lee, A. M., Ross, C. T., Zeng, B. B., and Singleton, S. F. (2005) A molecular target for suppression of the evolution of antibiotic resistance: inhibition of the *Escherichia coli* RecA protein by N(6)-(1-naphthyl)-ADP. *J. Med. Chem. 48*, 5408–5411.
26. Wigle, T. J., and Singleton, S. F. (2007) Directed molecular screening for RecA ATPase inhibitors. *Bioorg. Med. Chem. Lett. 17*, 3249–3253.
27. Qian, X., He, Y., Wu, Y., and Luo, Y. (2006) Asp302 determines potassium dependence of a RadA recombinase from *Methanococcus voltae*. *J. Mol. Biol. 360*, 537–547.
28. McRee, D. E. (1999) XtalView/Xfit—A versatile program for manipulating atomic coordinates and electron density. *J. Struct. Biol. 125*, 156–165.
29. Brunger, A. T., Adams, P. D., Clore, G. M., DeLano, W. L., Gros, P., Grosse-Kunstleve, R. W., Jiang, J. S., Kuszewski, J., Nilges, M., Pannu, N. S., Read, R. J., Rice, L. M., Simonson, T., and Warren, G. L. (1998) Crystallography & NMR system: A new software suite for macromolecular structure determination. *Acta Crystallogr., Sect. D: Biol. Crystallogr. 54* (Part 5), 905–921.
30. Kraulis, P. (1991) MOLSCRIPT: A program to produce both detailed and schematic plots of protein structures. *J. Appl. Crystallogr. 24*, 946–950.
31. Bacon, D. J., and Anderson, W. F. (1988) A fast algorithm for rendering space-filling molecule pictures. *J. Mol. Graphics 6*, 219–220.
32. Itaya, K., and Ui, M. (1966) A new micromethod for the colorimetric determination of inorganic phosphate. *Clin. Chim. Acta 14*, 361–366.
33. Qian, X., He, Y., Ma, X., Fodje, M. N., Grochulski, P., and Luo, Y. (2006) Calcium stiffens archaeal Rad51 recombinase from *Methanococcus voltae* for homologous recombination. *J. Biol. Chem. 281*, 39380–39387.
34. Shigeta, S., Mori, S., Yamase, T., and Yamamoto, N. (2006) Anti-RNA virus activity of polyoxometalates. *Biomed. Pharmacother. 60*, 211–219.
35. Sarafianos, S. G., Kortz, U., Pope, M. T., and Modak, M. J. (1996) Mechanism of polyoxometalate-mediated inactivation of DNA polymerases: an analysis with HIV-1 reverse transcriptase indicates specificity for the DNA-binding cleft. *Biochem. J. 319* (Part 2), 619–626.
36. Mecozzi, S., West, A. P., Jr., and Dougherty, D. A. (1996) Cation-pi interactions in aromatics of biological and medicinal interest: electrostatic potential surfaces as a useful qualitative guide. *Proc. Natl. Acad. Sci. U.S.A. 93*, 10566–10571.
37. Dougherty, D. A. (1996) Cation-pi interactions in chemistry and biology: a new view of benzene, Phe, Tyr, and Trp. *Science 271*, 163–168.